HHS Public Access

Author manuscript

Biomaterials. Author manuscript; available in PMC 2022 June 01.

Published in final edited form as:

Biomaterials. 2021 June ; 273: 120792. doi:10.1016/j.biomaterials.2021.120792.

A versatile photothermal vaccine based on acid-responsive glyco-nanoplatform for synergistic therapy of cancer

Yanan Gao[a], **Qingyu Zhao**[a], **Min Xiao**[a,b], **Xuefei Huang**[c], **Xuanjun Wu**[a,d,*]

[a]National Glycoengineering Research Center, Shandong Key Laboratory of Carbohydrate Chemistry and Glycobiology, NMPA Key Laboratory for Quality Research and Evaluation of Carbohydrate-based Medicine, Shandong University, Qingdao, Shandong, 266237, China

[b]State Key Laboratory of Microbial Technology, Shandong University, Qingdao, Shandong, 266237, China

[c]Departments of Chemistry and Biomedical Engineering, Institute for Quantitative Health Science and Engineering, Michigan State University, East Lansing, MI, 48824, United States

[d]Suzhou Research Institute, Shandong University, Suzhou, Jiangsu, 215123, China

Abstract

The race is on for therapeutic agents that stop cancer. An effective vaccine offers a safe and promising approach for cancer immunotherapy. However, substantial barriers to immunotherapy in cancer vaccines include the low immunogenicity of cancer antigens and the immunosuppression commonly present in solid tumors, resulting in significant challenges for developing a clinically effective cancer vaccine. Here, the state of the art of synergistic therapy, which includes the photothermal effect combined with immunotherapy, was investigated to target tumors. For the first time, indocyanine green (ICG, referred to as I), imiquimod (R837, referred to as R) and a foreign cytotoxic T lymphocyte antigen peptide (CTL-Ap, referred to as Ap) with the sequence of SIINFEKL from ovalbumin (OVA) were encapsulated by acetalated dextran (AcDEX) to form nanoparticles (NPs) averaging 92 nm in diameter as an immunogen. Administration of the resulting multifunctional vaccine I-R-Ap-AcDEX NPs enhanced antitumor cytotoxic T lymphocyte (CTL) immunotherapy. On the one hand, subcutaneous immunization of the NPs allows foreign Ap to enter the major histocompatibility complex class I (MHC-I) cross-presentation pathway of antigen-presenting cells, thereby presenting Ap and eliciting high levels of Ap-specific CTLs. On the other hand, intratumor/intravenous injections of the NPs allow foreign Ap to enter tumor cells and present Ap through the MHC-I cross-presentation pathway.

*Corresponding author. National Glycoengineering Research Center, Shandong University, Qingdao, Shandong 266237, China. xuanjun@sdu.edu.cn (X. Wu).

Credit author statement

Yanan Gao: Conceptualization, performing the experiments, formal analysis, writing original draft; **Qingyu Zhao:** Validation, formal analysis; **Min Xiao:** Resources, review; **Xuefei Huang:** Resources, review/editing; **Xuanjun Wu:** Conceptualization, project administration, methodology, resources, formal analysis, writing original draft & review/editing, funding acquisition.

Declaration of competing interest

The authors declare that they have no known competing financial interests or personal relationships that could have appeared to influence the work reported in this paper.

Appendix A. Supplementary data

Supplementary data to this article can be found online at https://doi.org/10.1016/j.biomaterials.2021.120792.

Ap-specific CTLs can kill Ap-presented tumor cells. Furthermore, the NPs generated near-infrared laser triggered the photothermal killing of tumor cells. To our knowledge, this is the first report of AcDEX NPs in antitumor photothermal therapy. Strikingly, systemic administration of the I-R-Ap-AcDEX NPs combined with near-infrared laser irradiation allowed for complete protection to mice from the tumors when applied to two non-OVA tumor models. This quite impressive result displays the great promise of synergistic therapy by the vaccine I-R-Ap-AcDEX NPs, an approach that harnesses the photothermal effect to boost antitumor immunotherapy.

Keywords

Cytotoxic T cells; Immunotherapy; Photothermal therapy; Nanoparticles; Cancer

1. Introduction

The development of successful cancer vaccines will be a massive leap for cancer prevention and treatment [1–4]. Cytotoxic T lymphocytes (CTLs) play a crucial role in exerting antitumor immune responses. Therefore, a promising direction for cancer vaccines is to focus on mobilizing antitumor CTL immunity [1,5–8]. To initiate CTL activation, exogenous antigens need to be presented on the major histocompatibility complex class I (MHC-I) molecules by antigen-presenting cells (APCs) [9]. However, under immune pressure from CTLs, tumor cells can decrease the levels of MHC-I expression, thus escaping immune surveillance [10,11].

A common strategy for eliciting potent CTL responses is to explore carriers such as inorganic nanoparticles [12–15], liposomes [16], protein particles [17], and polymer particles [8,18–23] to deliver antigens [24,25]. Among these carriers, the particles formed by acetalated dextran (AcDEX), a biodegradable polymer, have attracted much interest in cancer immunotherapy [26–30]. Compared to poly-(-lactic-co-glycolic acid) (PLGA), a gold standard carrier platform for antigen delivery [19–23,31–33], the AcDEX can elicit more robust cellular and humoral immune responses [28]. Besides, the AcDEX microparticles (MPs) can deliver an exogenous Ap from ovalbumin with the sequence of SIINFEKL to tumor tissues [34]. While immunization with Ap loaded AcDEX MPs could reduce the size of tumors, significant tumor growth was still observed in immunized animals. Thus, new strategies that could further improve the antitumor efficacy of immunotherapy are needed.

We have begun to investigate strategies for a multifunctional vaccine based on the AcDEX NPs. Co-delivery of antigens with adjuvants can markedly promote antitumor CTL responses [12,31–33,35]. Furthermore, synergistic combination therapies offer a tremendous promising treatment for cancer [36,37]. Among them, antitumor photothermal therapy is of much interest because of its unique advantages of precise spatial and temporal control, minimal invasiveness, and limited therapeutic resistance [38–40]. Compared with traditional chemotherapy, photothermal therapy is less damaging to healthy cells [40]. We hypothesize that antigen and adjuvant co-delivery combined with photothermal therapy, can achieve better antitumor therapeutic efficacy. To the best of our knowledge, the AcDEX NPs encapsulating photothermal agents for antitumor photothermal therapy have

not been investigated. Here we report for the first time that photothermal agent ICG (I), adjuvant R837 (R), and a foreign Ap can be co-encapsulated within the same AcDEX NP. Immunization with the resulting I-R-Ap-AcDEX NPs significantly improved antitumor efficacy when combined with near-infrared irradiation of tumors.

2. Experimental section

2.1. Synthesis of acetalated dextran (AcDEX) polymers

10 mL of dimethyl sulfoxide was added to a dried flask charged with dextran from *Leuconostoc mesenteroides* (molecular weight: 9–11 KDa, 1.00 g). 15.6 mg of Pyridinium *p*-toluenesulfonate (0.062 mmol) and 3.4 mL of 2-methoxypropene (37 mmol) were then added. The flask was placed by nitrogen protection. 10 min (for the synthesis of AcDEX1), 3 h (for the synthesis of AcDEX2) or 24 h (for the synthesis of AcDEX3) later, 1 mL of triethylamine (7 mmol) was added to quench the reaction. The acetalated dextran was precipitated in 100 mL of ultrapure water. The precipitate was followed by centrifugation at 12000 rpm for 20 min and washed thoroughly with ultrapure water (2 × 50 mL). By removing the supernatant after centrifugation, the precipitate was dried by lyophilization to afford AcDEX1, AcDEX2 and AcDEX3 polymers, which were characterized by ^{1}H NMR. ^{1}H NMR (600 MHz, $CDCl_3$) of AcDEX1: δ 1.40 (s, 5 H), 1.62 (m, 2 H), 3.25 (t, 2 H), 3.50 (d, 1 H), 3.60–4.15 (m, 3 H); ^{1}H NMR (600 MHz, $CDCl_3$) of AcDEX2: δ 1.39 (m, 18 H), 1.66 (d, 4 H), 2.62 (s, 1 H), 3.24 (m, 4 H), 3.52 (m, 2 H), 3.60–4.15 (m, 8 H), 5.13 (d, 2 H); ^{1}H NMR (600 MHz, $CDCl_3$) of AcDEX3: δ 1.40 (m, 10 H), 1.63 (d, 3 H), 3.24 (m, 2 H), 3.53 (m, 1 H), 3.60–4.15 (m, 5 H), 5.04 (m, 1 H).

2.2. Synthesis of I-R-Ap-AcDEX2 NPs

AcDEX2 NPs containing ICG, R837, and Ap were synthesized by a double emulsion method [26]. In brief, 20 mg of AcDEX2 in dichloromethane (1 mL) was added to 50 μL of dimethyl sulfoxide solution, which contains Ap (2 mg), R837 (2 mg) and ICG (2 mg). The mixture was emulsified by sonicating for 1 min (4 s on, 2 s off) on ice using a sonicator (SONICS VCX 500, with a duty cycle of 20%). And, the primary emulsion was added to 2 mL of poly(vinyl alcohol) (PVA, molecular weight: 13 000–23 000 g mol^{-1}) aqueous solution (3% w/w in ultrapure water). After sonicating for 1 min on ice, the resulting emulsion was added into 10 mL of PVA aqueous solution (0.3% w/w in ultrapure water) and stirred for 3 h. The NPs were isolated by centrifugation (12000 rpm, 20 min), washed with ultrapure water (3 × 20 mL), and lyophilized to afford I-R-Ap-AcDEX2 NPs. As a control, R-Ap-AcDEX2 NPs that did not contain ICG were synthesized using the same method as above omitting ICG. The NPs were characterized by transmission electron microscopy.

2.3. Quantification of encapsulated Ap, R837 and ICG in the NPs

To quantify the amounts of encapsulated Ap or/and R837 in the NPs, standard curves of Ap and R837 were generated from HPLC analysis (Figs. S3 and S5). In brief, various amounts of the NPs (2 mg) were hydrolyzed in 1 mL of 0.5% trifluoroacetic acid aqueous solution for 8 h and then analyzed by HPLC. The amounts of Ap and R837 were calculated from standard curves. The quantity of ICG in the NPs was determined from the standard curve of ICG generated from UV–Visible–NIR measurement at 790 nm (Fig. S6).

2.4. Degradation of AcDEX2 NPs, Ap and R837 release from I-R-Ap-AcDEX2 NPs

The solutions of AcDEX2 NPs (5 mg mL^{-1}) in PBS (0.1 M) with pH values of 7.4, 6.0 or 5.5 were incubated under room temperature (RT) and at 37 °C, respectively. UV–Visible measurements at 600 nm were performed every 1–4 h until 75 h. To test the release profiles of Ap and R837, I-R-Ap-AcDEX2 NPs (0.5 mg) were next suspended in 1 mL of 0.1 M PBS (pH 7.4 or pH 5.5) and kept at 37 °C. At selected time intervals (6–48 h), the suspension was centrifuged. Afterward, the pellets were hydrolyzed in 1 mL of 0.5% trifluoroacetic acid aqueous solution for 8 h, followed by HPLC analysis.

2.5. Determination of Ap presentation on MHC-I by tumor cells

EL4 lymphoma cells (5×10^5) were cultured overnight and incubated with free Ap (1 μg) or the NPs containing 1 μg of Ap for 6 h. After washing with phosphate-buffered saline (PBS) containing 1% fetal bovine serum (FBS) and 0.1% NaN_3 (referred to as the buffer), the cells were stained with PE-labeled anti-mouse H-$2K^b$/SIINFEKL antibody for 30 min in the buffer on ice, washed with the buffer, and then imaged by a confocal microscope (Fig. 4a). For flow cytometry analysis, EL4 cells (5×10^5) were cultured overnight and then incubated with free Ap (1–1000 ng) or the NPs containing the same amounts of Ap for 6 h. After washing with the buffer, the cells were stained with PE-labeled anti-mouse H-$2K^b$/SIINFEKL antibody for 30 min in the buffer on ice. Then, the cells were washed and analyzed by flow cytometry (Fig. 4b).

2.6. B3Z T cell activation study

EL4 cells (5×10^4) or BMDCs (5×10^4) were respectively pulsed with free Ap or the NPs (1–1000 ng). After 18 h, B3Z T cells (3×10^5) were added and then cultured for 16 h. Afterward, the medium was gently removed by centrifugation at 2500 rpm for 5 min. Then, 100 μL of CPRG solution (90 mg of $MgCl_2$, 9.1 mg of CPRG, and 0.125 mg of NP40 in 100 mL PBS) was added. 6 h later, UV–visible absorbance at 595 nm was recorded. The assay was performed in three replicates.

2.7. In vivo CTL activity study

C57BL/6 mice were subcutaneously immunized once with PBS, free Ap, Ap-AcDEX2 NPs or I-R-Ap-AcDEX2 NPs under the scruff. The injection amounts of Ap were normalized to 30 μg. 7-day later, splenocytes from untreated mice were harvested, and half of the cells (5×10^7, 5 mL) were pulsed with 1 μg mL^{-1} of Ap for 1 h. The Ap pulsed splenocytes were supplemented with 10 μM of carboxyfluorescein succinimidyl ester (referred to as $CFSE^{hi}$), and no Ap pulsed splenocytes were supplemented with 1 μM of CFSE (referred to as $CFSE^{lo}$). Then, a mixture of $CFSE^{lo}$ and Ap pulsed $CFSE^{hi}$ splenic cells (1:1, 0.1 mL, 2×10^6 cells) was injected intravenously to PBS, free Ap, or the NPs immunized mice. 24 h later, spleen cells were collected, and 7-AAD (10 μg mL^{-1}) was added to the single suspension. The number of viable $CFSE^{hi}$ and $CFSE^{lo}$ cells were determined by flow cytometry. The changes in the ratio of $CFSE^{hi}$ to $CFSE^{lo}$ were analyzed from the FITC-FSC plot to evaluate target cell viability.

2.8. In vitro photothermal performances

An 808 nm fiber-coupled NIR laser (MW-GX-808/1–5000 mW, Changchun Laser Technology Co., Ltd. Jilin, China) was employed in the experiments. Ultrapure water was spiked with ICG or I-R-Ap-AcDEX2 NPs at increasing concentrations (0–50 ppm). The solution was irradiated with the 808 nm laser (1 W cm^{-2}) for 10 min, and the temperature of the solution was recorded over irradiation time.

2.9. In vitro photothermal killing of tumor cells

EL4 cells (1×10^5 cells per well) were cultured in a 96-well plate overnight. The cells were supplemented with ICG (0–20 ppm) or I-R-Ap-AcDEX2 NPs (internal ICG concentrations of 0–20 ppm) for 4 h, and irradiated with the 808 nm laser (1 W cm^{-2}) for 10 min then re-cultured for 12 h. After rinsing with PBS, these cells were co-stained with propidium iodide (PI) and Calcein AM for 30 min. After washing with PBS, the cells were imaged by fluorescence microscopy.

2.10. Determination of $CD8^+$ T cell infiltration in the tumor

C57BL/6 mice were subcutaneously injected with EL4 cells on day 0, followed by subcutaneous injection of I-R-Ap-AcDEX2 NPs under the scruff on day 1. On day 7, mice were intratumorally injected with I-R-Ap-AcDEX2 NPs, and the tumors were irradiated with the 808 nm laser at the power of 0, 0.1, 0.3 or 1 W cm^{-2}, respectively. The injection amounts of Ap were normalized to 30 μg. On day 8, the tumor tissues were removed from mice, and single-cell suspensions were generated. The cells were stained with FITC-labeled anti-mouse CD8α antibody (clone 53–6.7, BioLegend) for 30 min in the buffer on ice according to the manufacturer's instructions. After washing with the buffer, the cells were analyzed by flow cytometry.

2.11. Illumination of subcutaneous tumors with I-R-Ap-AcDEX2 NPs

C57BL/6 mice were xenografted by subcutaneous injections of EL4 cells (1×10^5). At 7 days after the transplantation, I-R-Ap-AcDEX2 NPs and free ICG were respectively injected into tumor-bearing mice via the tail vein. The injection amounts of ICG were normalized to 30 μg. At 0–22 h following injection, the mice were analyzed for whole-body NIR fluorescence imaging.

2.12. In vivo combined immuno-photothermal therapy of tumor

For local administration, C57BL/6 mice were subcutaneously inoculated with EL4 cells (2×10^5) on day 0, and subcutaneously injected on day 1 with 0.1 mL of PBS, I-R-Ap-AcDEX2 NPs, R-Ap-AcDEX2 NPs or I-AcDEX2 NPs. All vaccines injected have the same dose of Ap (30 μg). Then, a total of 3 injections with 0.1 mL of PBS, I-R-Ap-AcDEX2 NPs or I-AcDEX2 NPs were respectively given intratumorally on days 7, 10 and 12, with a dose of 30 μg Ap. For 808 nm laser-treated groups, mice after injection of I-R-Ap-AcDEX2 NPs or I-AcDEX2 NPs only on day 7 were irradiated with the NIR (808 nm) laser (1.0 W cm^{-2}, 3 min).

For systemic administration, C57BL/6 female mice were injected subcutaneously with EL4 cells (1×10^5) on day 0, subcutaneously immunized on day 1 with PBS or the NPs, intravenously given a total of 3 injections with PBS or the NPs on days 7, 10 and 13, respectively. For laser-irradiated groups, the mice treated with PBS, I-AcDEX2 NPs, or I-R-Ap-AcDEX2 NPs were irradiated with the 808 nm laser (1.0 W cm^{-2}, 3 min) on days 7, 10 and 13 at 2 h following injection of the NPs or PBS in mice. On days 20, 27, 34, 41 and 48, five more intravenous injections of I-R-Ap-AcDEX2 NPs plus laser irradiations (1.0 W cm^{-2}, 3 min) were performed in mice within the group (I-R-Ap-AcDEX2 NPs plus Laser). Tumor volume was calculated with the formula: Volume (mm^3) = 1/2 (length × width × height) [41].

3. Results and discussion

3.1. Optimization of the AcDEX system

The AcDEX NPs were synthesized through the acetal formation between free hydroxyl groups of the dextran (molecular weight: 9–11 kDa) and 2-methoxypropene with an acid catalyst. The kinetically favorable acyclic acetals were formed initially followed by the thermodynamically more stable cyclic acetals [42]. Compared to cyclic acetals, acyclic acetals are more easily degraded by acid hydrolysis [43]. Therefore, by judiciously choosing the reaction time for acetalization, the ratios of acyclic/cyclic acetals could be controlled, resulting in polymers with varying degradation rates.

To develop a structurally optimized AcDEX system for Ap delivery, AcDEX1, AcDEX2, and AcDEX3 polymers were synthesized (Scheme 1a) by controlling the acetalization time at 10 min, 3 h, and 24 h respectively. The structures of these polymers were characterized by ^{1}H NMR (Fig. S1). The encapsulation of Ap (SIINFEKL) into the NPs was carried out by double emulsion technology [26]. The resulting particles were isolated by centrifugation and dried by lyophilization to yield Ap-AcDEX1 NPs, Ap-AcDEX2 NPs, and Ap-AcDEX3 NPs (Scheme 1a). Furthermore, PLGA is a commonly used carrier for antigen delivery [19–23,31–33]. To benchmark the performance of our AcDEX NPs for Ap delivery, Ap-PLGA NPs have been synthesized by encapsulating Ap in PLGA as a control (Scheme 1b).

Transmission electron microscopy (TEM) images of these NPs showed the average diameters of Ap-AcDEX1 NPs, Ap-AcDEX2 NPs, Ap-AcDEX3 NPs, and Ap-PLGA NPs were 116 nm, 136 nm, 165 nm, and 132 nm (Fig. S2) respectively. The Ap encapsulated levels in the NPs were detected by high-performance liquid chromatography (HPLC) quantification after dissembling the NPs with a 0.5% trifluoroacetic acid aqueous solution. HPLC analysis showed the amounts of encapsulated Ap by Ap-AcDEX1 NPs, Ap-AcDEX2 NPs, Ap-AcDEX3 NPs, and Ap-PLGA NPs were measured reproducibly to be 50 μg, 50 μg, 30 μg and 30 μg of peptide per mg of NPs respectively (Tab. S1).

As a proof of concept, EL4 lymphoma cells, which express MHC-I on the cell surface, were selected for cell studies. Ap encapsulated in AcDEX particles can be loaded on MHC-I by EL4 cells [34]. To test whether CTLs could recognize Ap presented tumor cells, we performed an *in vitro* CTL activation study using B3Z $CD8^+$ T cell hybridoma assay [44,45]. B3Z T cells express T cell receptors specific for the complexes of SIINFEKL

peptide (Ap) and MHC-I H-2K^b molecule. Upon combination of its T cell receptors by Ap/MHC-I complexes, B3Z T cells can be activated to secret β-galactosidase, which cleaves CPRG to produce a colorimetric readout. To perform B3Z assay, EL4 cells were spiked with free Ap, Ap-AcDEX1 NPs, Ap-AcDEX2 NPs, Ap-AcDEX3 NPs, Ap-PLGA NPs or Ap mixed with empty AcDEX2 NPs. The resulting EL4 cells were co-cultured with B3Z T cells, and CPRG was added. Incubation of EL4 cells with Ap-AcDEX2 NPs generated the highest activation of B3Z T cells at equivalent Ap concentrations (Fig. 1). Encapsulation of antigens in carriers could realize an optimal CTL activation by sequestering antigens until they reach the target cells, delivering them to specific types of cells, and contributing to their presentation at appropriate rates via the desired pathways [28]. Thus, in our study, Ap-AcDEX2 NPs displayed more than a tenfold increase in B3Z activation compared to free Ap. Next, different activation effects were observed among Ap-AcDEX1–3 NPs in B3Z T cell assay owing to polymers AcDEX1–3 with varying degradation rates. Furthermore, a comparison of Ap-AcDEX NPs with Ap-PLGA NPs showed that AcDEX2 enhanced MHC-I antigen cross-presentation with the most robust B3Z activation within the groups, indicating the enormous potential of AcDEX2 for further vaccine design.

3.2. Design and synthesis of the I-R-Ap-AcDEX2 NPs

For developing a new generation AcDEX based vaccine, the I-R-Ap-AcDEX2 NPs composed of ICG, R837, Ap, and AcDEX2 were designed (Fig. 2). R837, a Toll-like receptor 7 (TLR-7) ligand, is known to activate immunity potently [46,47]. The co-delivery of R837 and antigen can lead to significant increases in immune responses [46]. Furthermore, ICG, an NIR agent approved by the U.S. FDA, has been actively investigated for human clinical NIR cancer imaging and photothermal therapy [48–52]. We envision that the incorporation of ICG and R837 into our Ap-AcDEX2 NPs can potentiate the immune system and delay tumor growth by combining immune activation and photothermal therapy.

The I-R-Ap-AcDEX2 NPs were prepared by ultrasonic emulsification and evaporation in the presence of ICG, R837, Ap, and AcDEX2. TEM images showed the average diameter of I-R-Ap-AcDEX2 NPs was 92 nm (Fig. S4). The amounts of Ap, R837, and ICG encapsulated by I-R-Ap-AcDEX2 NPs were determined to be 30 μg of Ap, 60 μg of R837, and 30 μg of ICG per mg of NPs (Tab. S1). We synthesized several I-R-Ap-AcDEX2 NPs and found that the particle size and Ap content of each batch were identical (data not shown), indicating the NP preparation procedure was highly reproducible. In parallel, R-Ap-AcDEX2 NPs were also prepared as ICG-free control. The amounts of Ap and R837 encapsulated by R-Ap-AcDEX2 NPs were determined to be 50 μg of Ap and 60 μg of R837 per mg of NPs (Tab. S1).

To test the pH responsiveness, the AcDEX2 NPs were dispersed in PBS (0.1 M) with pH values of 7.4, 6.0, or 5.5 under RT and 37 °C, respectively. UV–Visible diffraction at 600 nm of the NPs solution was monitored. When spiked into PBS (0.1 M) at pH 7.4 and 6.0, tiny absorbance changes were observed over 75 h at RT or 37 °C (Fig. 3a). In contrast, the NPs gradually degraded in PBS at pH 5.5 over 20 h owing to the cleavage of the acetal bond by acid hydrolysis. Furthermore, degradation of the NPs was promoted by increasing the temperature from RT to physiological temperature of 37 °C (Fig. 3a), readily

leading to improved release of encapsulated components. Subsequently, the release rates of encapsulated Ap and R837 in I-R-Ap-AcDEX2 NPs were evaluated after incubation of the NPs in PBS with pH 7.4 or pH 5.5 at 37 °C. At pH 7.4, the spontaneous release rates of Ap and R837 from the NPs were slow (Fig. 3b and c). In contrast, the release rates of them were significantly increased at pH 5.5 (Fig. 3b and c). This indicates that Ap and R837 would not be prematurely released in the close to neutral extracellular environment. Upon uptake by cells, the late endosomes and lysosomes' acidic environment could presumably promote Ap's release from the NPs, facilitating MHC-I presentation of the Ap. To confirm this, we next studied the release of Ap within the tumor cells. FITC-labeled SIINFEKL (referred to as ^{FITC}Ap) was used instead of Ap for visualizing Ap in cells. Interestingly, the tumor cells treated with I-R-^{FITC}Ap-AcDEX2 NPs showed strong FITC fluorescence in the whole cells, not limited to lysosomes (Fig. S7), suggesting the successful release of Ap from the NPs in cells. Besides, Ap delivered by the NPs increase cellular uptake, which could produce superior MHC-I presentation (Fig. S7).

3.3. Immunological evaluation of the I-R-Ap-AcDEX2 NPs

In our design, if foreign Ap can be delivered to the tumor, it can potentially lead to the presentation of foreign Ap on tumor cells, producing Ap-labeled tumor cells as CTLs targets. Therefore, we next tested Ap presentation on MHC-I by tumor cells. EL4 tumor cells were incubated with free Ap, Ap-AcDEX2 NPs, I-R-Ap-AcDEX2 NPs or R-Ap-AcDEX2 NPs, stained with PE-labeled anti-mouse H-2K^b/SIINFEKL antibody, and analyzed by confocal microscopy (Fig. 4a) or flow cytometry (Fig. 4b). Incubation of EL4 cells with I-R-Ap-AcDEX2 NPs or R-Ap-AcDEX2 NPs led to much-increased cellular fluorescence intensities relative to those with free Ap and Ap-AcDEX2 NPs (Fig. 4a and b). This validates the significant importance of R837 for enhancing MHC-I antigen cross-presentation. To further confirm this, an extra group of I-Ap-AcDEX2 NPs was also synthesized for comparison. As shown in Fig. S8, I-Ap-AcDEX2 NPs exhibited lower levels of MHC-I cross-presentation than I-R-Ap-AcDEX2 NPs, further validating the importance of R837. Furthermore, similar results were also observed in the study of MC38 colon carcinoma cells (Fig. S9), suggesting the generality of the I-R-Ap-AcDEX2 NPs, which could be applied to multiple types of tumor cells.

Inspired by superior MHC-I presentation of Ap delivered by these NPs, we performed *in vitro* CTL assay to access their abilities in activating B3Z T cells. EL4 cells were incubated with free Ap, Ap-AcDEX2 NPs, R-Ap-AcDEX2 NPs, or I-R-Ap-AcDEX2 NPs, then co-cultured with B3Z T cells followed by the addition of CPRG. Compared with Ap-AcDEX2 NPs, the R837 encapsulated NPs allowed a much higher activation of B3Z T cells (Fig. 4c). EL4 cells treated with R-Ap-AcDEX2 NPs generated strong B3Z activation comparable to that of I-R-Ap-AcDEX2 NPs, indicating no negative impacts by ICG on CTL activation. Besides having an excellent immunostimulant effect on immune cells, R837 can also significantly promote TLR-7 activation of tumor cells [53]. Thus, it was reasonable that the incorporation of R837 in the AcDEX NPs effectively enhanced the cross-presentation of Ap on tumor cells.

To investigate the induction of activated CTLs, we next studied the presentation of Ap by bone marrow dendritic cells (BMDCs), which is a critical step in generating CTLs. As shown in Fig. 5a, incubation of I-R-Ap-AcDEX2 NPs or R-Ap-AcDEX2 NPs with BMDCs induced activation of B3Z T cells more than the other control groups, consistent with antibodies staining data mentioned in Fig. 4, confirming the significant importance of R837 in the AcDEX NP formulation for CTL induction. Furthermore, CTL activation by I-R-Ap-AcDEX2 NPs *in vivo* was evaluated next. Mice were vaccinated with I-R-Ap-AcDEX2 NPs by one injection, and the resulting CTL activities of immunized mice were determined by the *in vivo* CFSE assay [54]. As shown in Fig. 5b, I-R-Ap-AcDEX2 NPs vaccination by subcutaneous route activated higher levels of Ap-specific CTLs than other groups, leading to significant death of Ap containing target cells. However, intravenous administration of I-R-Ap-AcDEX2 NPs induced low CTL activation (Fig. S10). Thus, the subcutaneous route was used for CTL induction in further studies.

3.4. In vitro photothermal activities of the I-R-Ap-AcDEX2 NPs

The incorporation of ICG endows I-R-Ap-AcDEX2 NPs with remarkable near-infrared (NIR) absorption (Fig. 6a), bestowing excellent photothermal conversion efficiency to the NPs. Under 808 nm laser irradiation, the temperature of I-R-Ap-AcDEX2 NPs solution rose faster than that of ICG solution with the same concentration (Fig. 6b and c), suggesting an enhanced photothermal effect of ICG in the NPs. The photostabilities of the I-R-Ap-AcDEX2 NPs and free ICG were also tested under 808 nm laser on/off cycle irradiation. Strikingly, I-R-Ap-AcDEX2 NPs exhibited much enhanced photostability than free ICG likely due to the protection of ICG from photobleaching by the NPs (Fig. 6d), which implies antitumor photothermal therapy could be improved by ICG encapsulated in the AcDEX system.

Next, the photothermal abilities of I-R-Ap-AcDEX2 NPs and free ICG for killing cancer cells were investigated. After incubation with I-R-Ap-AcDEX2 NPs or free ICG for 4 h, the EL4 cells were treated with the 808 nm laser at a power density of 1 W cm^{-2} for 10 min (Fig. 6e), then co-stained with propidium iodide (PI, for dead cells, red fluorescence) and calcein-AM (for live cells, green fluorescence). As shown in Fig. 6e, 10 ppm free ICG was needed to kill all EL4 cells after laser irradiation. In comparison, similar photo-toxicities to cancer cells were observed with the nanoparticles containing only 2 ppm of ICG. These results proved excellent photothermal therapy efficiency of the I-R-Ap-AcDEX2 NPs in killing cancer cells.

The photothermal performance of the NPs in the EL4 tumor-bearing mice was also tested. IR thermal images of EL4 tumor-bearing mice intratumorally injected with I-R-Ap-AcDEX2 NPs showed its local temperature of the tumor rapidly increased to 44 °C under 808 nm laser irradiation for 3 min (Fig. S11). This local mild hyperthermia enables tumor cell killing [55]. In addition, mild hyperthermia is less harmful to healthy cells than to tumor cells because healthy cells can tolerate higher temperatures. Most importantly, the latest study has shown that mild hyperthermia effectively helps CAR-T cells attack tumors and significantly improves CAR-T cells' antitumor efficacy [56]. Thus, it can be inferred that mild hyperthermia can potentially promote the anti-tumor efficacy of CTL immunotherapy.

3.5. Combined immuno-photothermal therapy of tumor enabled by the I-R-Ap-AcDEX2 NPs

With superior CTL activation and photothermal properties by the I-R-Ap-AcDEX2 NPs, we next evaluate the antitumor activities of combining the photothermal effect and CTL immunotherapy. Besides directly killing tumor cells, mild hyperthermia can change tumors' structures, promoting the infiltration of immune cells into tumors [56]. To test that, C57BL/6 mice bearing EL4 cells were subcutaneously immunized with I-R-Ap-AcDEX2 NPs. After 6 days, the mice were intratumorally injected with I-R-Ap-AcDEX2 NPs, followed by the 808 nm laser irradiation at the power of 0, 0.1, 0.3 or 1.0 W cm^{-2}, respectively. As shown in Fig. 7a, photothermal therapy with laser irradiation at 1.0 W cm^{-2} significantly increased the percentages of $CD8^+$ T cells in tumors, suggesting that the infiltration of $CD8^+$ T cells into tumors was enhanced, which would improve antitumor CTL immunotherapy. And thus, the irradiation condition (1.0 W cm^{-2}) was established for further studies.

Subsequently, we evaluated the ability of I-R-Ap-AcDEX2 NPs to offer tumor protection *in vivo*. C57BL/6 mice were subcutaneously implanted with EL4 cells on day 0, followed by subcutaneous injection on day 1 with various nanoparticle formulations or PBS. From day 7, the mice were intratumorally given a total of 3 doses with various NPs or PBS, and the growth of the tumor was monitored. Laser irradiations were performed on day 7. As shown in Fig. 7b, the two groups receiving R-Ap-AcDEX2 NPs and I-R-Ap-AcDEX2 NPs injections respectively, at the same total dose of Ap led to a significant reduction in tumor sizes compared with the mock group receiving PBS injection, indicating the superior induction of antitumor CTL responses by R-Ap-AcDEX2 NPs and I-R-Ap-AcDEX2 NPs. Also, laser irradiation alone did not have much effect on tumor growth. The most effective reduction of tumor growth was observed with I-R-Ap-AcDEX2 NPs combined with laser irradiation on the tumor. This suggests that CTL immunotherapy and photothermal therapy by I-R-Ap-AcDEX2 NPs can significantly improve the tumor protection effect. Furthermore, an essential criterion for designing vaccines is that they should not cause undesired side effects. In our study, no noticeable side effect of the NPs was observed for the treated mice by histological analysis (Fig. 7c), confirming this vaccine's potency and safety for future clinical translation.

Finally, we would like to investigate the possibility of realizing the synergistic therapy of tumors by intravenous systemic administration of the I-R-Ap-AcDEX2 NPs. To begin with, we evaluated the NPs for their efficacy in illuminating subcutaneous tumors in mice. Remarkably, I-R-Ap-AcDEX2 NPs exhibited a more favorable accumulation in the tumor than free ICG likely due to the well-known enhanced permeability and retention (EPR) effect by NPs (Fig. 8a). This indicates that the NPs have great potential for systemic administration. To confirm that, a further tumor challenge study was performed. C57BL/6 mice were subcutaneously inoculated with EL4 cells, subcutaneously immunized with PBS or the NPs next day, and maintained for 6 days development of tumor xenografts. PBS or the NPs were intravenously injected into the tumor-bearing mice by tail vein on days 7, 10 and 13, respectively (Fig. 8b). Then the tumors were irradiated with the 808 nm laser (1.0 W cm^{-2}, 3 min) after 2 h of injection of the NPs or PBS in mice. In parallel, PBS or the NPs treated mice without laser irradiation were prepared as control groups.

As shown in Fig. 8c, I-AcDEX2 NPs injection, plus laser irradiation were slightly slowing down tumor growth. In contrast, the group receiving I-R-Ap-AcDEX2 NPs injection led to a significant reduction in tumor sizes, indicating the superiority of the I-R-Ap-AcDEX2 NPs. Interestingly, systemic treatment increased the percentages of MHC-I^+ cells and $CD8^+$ T cells infiltrating the EL4 tumor (Fig. S13), as well as upregulated the expression of MHC-I on splenic immune cells (Fig. S14). Most importantly, the combination of I-R-Ap-AcDEX2 NPs with laser irradiation allowed for complete protection to mice from the EL4 tumor for 80 days (Fig. 8c and d). To further see the effect of R837 with photothermal therapy, a control group that has everything except the Ap was also evaluated for comparison. As shown in Fig. S15, the combination of I-R-AcDEX2-NPs with laser irradiation showed poor tumor protection, validating the significant importance of Ap for anti-tumor CTL immunity. Besides, the combination of I-R-Ap-AcDEX2 NPs with laser irradiation also allowed for complete protection to mice from the MC38 colon carcinoma, a non-OVA solid tumor model (Fig. S16), confirming the generality of this combination therapy. Furthermore, no adverse autoimmune complications were observed in all mice.

4. Conclusion

In summary, we have reported a new therapeutic vaccine I-R-Ap-AcDEX2 NPs, comprising ICG, R837, an exogenous Ap antigen (SIINFEKL) and acetalated dextran (AcDEX2), which induced robust anti-tumor CTL responses and efficient antitumor photothermal effect. Upon incubation, the NPs were taken up by tumor cells, where Ap could be cross-presented on MHC-I, leading to Ap labeled tumor cells, which became CTL targets. The successful cell surface display of Ap on MHC-I and the production of potent SIINFEKL-specific CTLs enabled by the I-R-Ap-AcDEX2 NPs allows for superior antitumor CTL immunotherapy, which offers a broadly applicable strategy for cancer treatment. Furthermore, this is the first report using the AcDEX system for anti-tumor photothermal therapy. By combining photothermal therapy and CTL immunotherapy, complete protection of mice from tumor growth has been achieved, highlighting its high translation potential.

Supplementary Material

Refer to Web version on PubMed Central for supplementary material.

Acknowledgment

This work was supported by grants from the Qilu Young Scholar Fund of Shandong University, the National Natural Science Foundation of China (22007058), the Natural Science Foundation of Shandong Province (ZR2020QB165), the Natural Science Foundation of Jiangsu Province (BK20200236), the State Key Laboratory of Microbial Technology Open Projects Fund (M2020-02), and the National Cancer Institute (R01 CA225105). We want to thank Prof. Chuangnian Zhang and Prof. Xiaoli Wang (Institute of Biomedical Engineering, Chinese Academy of Medical Sciences & Peking Union Medical College) to provide us B3Z T cells.

References

[1]. Tanyi JL, Bobisse S, Ophir E, Tuyaerts S, Roberti A, Genolet R, Baumgartner P, Stevenson BJ, Iseli C, Dangaj D, Czerniecki B, Semilietof A, Racle J, Michel A, Xenarios I, Chiang C, Monos DS, Torigian DA, Nisenbaum HL, Michielin O, June CH, Levine BL, Powel DJ, Gfeller D, Mick R, Dafni U, Zoete V, Harari A, Coukos G, Kandalaft LE, Personalized cancer vaccine

effectively mobilizes antitumor T cell immunity in ovarian cancer, Sci. Transl. Med10 (436) (2018), eaao5931. [PubMed: 29643231]

[2]. Melero I, Gaudernack G, Gerritsen WR, Huber C, Parmiani G, Scholl S, Thatcher N, Wagstaff J, Zielinski C, Faulkner I, Mellstedt H, Therapeutic vaccines for cancer: an overview of clinical trials, Nat. Rev. Clin. Oncol11 (9) (2014) 509–524. [PubMed: 25001465]

[3]. Van Der Burg SH, Arens R, Ossendorp F, Van Hall T, Melief CJM, Vaccines for established cancer: overcoming the challenges posed by immune evasion, Nat. Rev. Canc16 (4) (2016) 219–233.

[4]. Romero P, Banchereau J, Bhardwaj N, Cockett M, Disis ML, Dranoff G, Gilboa E, Hammond SA, Hershberg R, Korman AJ, Kvistborg P, Melief C, Mellman I, Palucka AK, Redchenko I, Robins H, Sallusto F, Schenkelberg T, Schoenberger S, Sosman J, Türeci Ö, Van Den Eynde B, Koff W, Couko G, The human vaccines project: a roadmap for cancer vaccine development,, Sci. Transl. Med8 (334) (2016) 334ps9.

[5]. Bae J, Parayath N, Ma WX, Amiji M, Munshi N, Anderson KC, BCMA peptide-engineered nanoparticles enhance induction and function of antigen-specific CD8(+) cytotoxic T lymphocytes against multiple myeloma: clinical applications, Leukemia34 (1) (2020) 210–223. [PubMed: 31427721]

[6]. Kuai R, Ochyl LJ, Bahjat KS, Schwendeman A, Moon JJ, Designer vaccine nanodiscs for personalized cancer immunotherapy, Nat. Mater16 (4) (2016) 489–498. [PubMed: 28024156]

[7]. Galea-Lauri J, Darling D, Mufti G, Harrison P, Farzaneh F, Eliciting cytotoxic T lymphocytes against acute myeloid leukemia-derived antigens: evaluation of dendritic cell–leukemia cell hybrids and other antigen-loading strategies for dendritic cell-based vaccination, Cancer Immunol. Immunother51 (6) (2002) 299–310. [PubMed: 12111118]

[8]. Luo M, Wang H, Wang Z, Cai H, Lu Z, Li Y, Du M, Huang G, Wang C, Chen X, Porembka MR, Lea J, Frankel AE, Fu Y-X, Chen ZJ, Gao J, A STING-activating nanovaccine for cancer immunotherapy, Nat. Nanotechnol12 (7) (2017) 648–654. [PubMed: 28436963]

[9]. Villadangos JA, Schnorrer P, Intrinsic and cooperative antigen-presenting functions of dendritic-cell subsets in vivo, Nat. Rev. Immunol7 (7) (2007) 543–555. [PubMed: 17589544]

[10]. Bubeník J, MHC class I down-regulation: tumour escape from immune surveillance?Int. J. Oncol25 (2) (2004) 487–491. [PubMed: 15254748]

[11]. Khanna R, Tumour surveillance: missing peptides and MHC molecules, Immunol. Cell Biol76 (1) (1998) 20–26. [PubMed: 9553772]

[12]. Cha BG, Jeong JH, Kim J, Extra-large pore mesoporous silica nanoparticles enabling co-delivery of high amounts of protein antigen and Toll-like receptor 9 agonist for enhanced cancer vaccine efficacy, ACS Cent. Sci4 (4) (2018) 484–492. [PubMed: 29721531]

[13]. Hassan HAFM, Smyth L, Wang JTW, Costa PM, Ratnasothy K, Diebold SS, Lombardi G, Al-Jamal KT, Dual stimulation of antigen presenting cells using carbon nanotube-based vaccine delivery system for cancer immunotherapy, Biomaterials104 (2016) 310–322. [PubMed: 27475727]

[14]. Kang S, Ahn S, Lee J, Kim JY, Choi M, Gujrati V, Kim H, Kim J, Shin E-C, Jon S, Effects of gold nanoparticle-based vaccine size on lymph node delivery and cytotoxic T-lymphocyte responses, J. Contr. Release256 (2017) 56–67.

[15]. Zhang P, Chiu Y-C, Tostanoski LH, Jewell CM, Polyelectrolyte multilayers assembled entirely from immune signals on gold nanoparticle templates promote antigen-specific T cell response, ACS Nano9 (6) (2015) 6465–6477. [PubMed: 26035231]

[16]. Chen W, Huang L, Induction of cytotoxic T-lymphocytes and antitumor activity by a liposomal lipopeptide vaccine, Mol. Pharm5 (3) (2008) 464–471. [PubMed: 18266319]

[17]. Neek M, Kim TI, Wang S-W, Protein-based nanoparticles in cancer vaccine development, Nanomedicine15 (1) (2019) 164–174. [PubMed: 30291897]

[18]. Brubaker CE, Panagiotou V, Demurtas D, Bonner DK, Swartz MA, Hubbell JA, A cationic micelle complex improves CD8+ T cell responses in vaccination against unmodified protein antigen, ACS Biomater. Sci. Eng2 (2) (2016) 231–240. [PubMed: 33418636]

[19]. Egilmez NK, Egilmez NK, Jong YS, Jong YS, Sabel MS, Sabel MS, Jacob JS, Jacob JS, Mathiowitz E, Mathiowitz E, Bankert RB, Bankert RB, In situ tumor vaccination with

interleukin-12-encapsulated biodegradable microspheres: induction of tumor regression and potent antitumor immunity, Canc. Res60 (14) (2000) 3832–3837.

[20]. Jahan ST, Sadat SMA, Yarahmadi M, Haddadi A, Potentiating antigen specific immune response by targeted delivery of the PLGA-based model cancer vaccine, Mol. Pharm16 (2) (2019) 498–509. [PubMed: 30477303]

[21]. Rietscher R, Schröder M, Janke J, Czaplewska J, Gottschaldt M, Scherließ R, Hanefeld A, Schubert US, Schneider M, Knolle PA, Lehr C-M, Antigen delivery via hydrophilic PEG-b-PAGE-b-PLGA nanoparticles boosts vaccination induced T cell immunity, Eur. J. Pharm. Biopharm102 (2016) 20–31. [PubMed: 26940132]

[22]. Xia Y, Wei J, Du Y, Wan T, Ma X, An W, Guo A, Miao C, Yue H, Li S, Cao X, Su Z, Ma G, Exploiting the pliability and lateral mobility of Pickering emulsion for enhanced vaccination, Nat. Mater17 (2) (2018) 187–194. [PubMed: 29300052]

[23]. Zhang Z, Tongchusak S, Mizukami Y, Kang YJ, Ioji T, Touma M, Reinhold B, Keskin DB, Reinherz EL, Sasada T, Induction of anti-tumor cytotoxic T cell responses through PLGA-nanoparticle mediated antigen delivery, Biomaterials32 (14) (2011) 3666–3678. [PubMed: 21345488]

[24]. Chesson CB, Ekpo-Otu S, Endsley JJ, Rudra JS, Biomaterials-based vaccination strategies for the induction of CD8+T cell responses, ACS Biomater. Sci. Eng3 (2) (2017) 126–143. [PubMed: 33450791]

[25]. Shao K, Singha S, Clemente-Casares X, Tsai S, Yang Y, Santamaria P, Nanoparticle-based immunotherapy for cancer, ACS Nano9 (1) (2015) 16–30. [PubMed: 25469470]

[26]. Bachelder EM, Beaudette TT, Broaders KE, Dashe J, Fŕechet JMJ, Acetal-derivatized dextran: an acid-responsive biodegradable material for therapeutic applications, J. Am. Chem. Soc130 (32) (2008) 10494–10495. [PubMed: 18630909]

[27]. Bachelder EM, Pino EN, Ainslie KM, Acetalated dextran: a tunable and acid-labile biopolymer with facile synthesis and a range of applications, Chem. Rev117 (3) (2017) 1915–1926. [PubMed: 28032507]

[28]. Broaders KE, Cohen JA, Beaudette TT, Bachelder EM, Jean MJF, Acetalated dextran is a chemically and biologically tunable material for particulate immunotherapy, Proc. Natl. Acad. Sci. U. S. A106 (14) (2009) 5497–5502. [PubMed: 19321415]

[29]. Collier MA, Junkins RD, Gallovic MD, Johnson BM, Johnson MM, Macintyre AN, Sempowski GD, Bachelder EM, Ting JPY, Ainslie KM, Acetalated dextran microparticles for codelivery of STING and TLR7/8 agonists, Mol. Pharm15 (11) (2018) 4933–4946. [PubMed: 30281314]

[30]. Cui L, Cohen JA, Broaders KE, Beaudette TT, Fréchet JMJ, Mannosylated dextran nanoparticles: a pH-sensitive system engineered for immunomodulation through mannose targeting, Bioconjugate Chem. 22 (5) (2011) 949–957.

[31]. Dölen Y, Kreutz M, Gileadi U, Tel J, Vasaturo A, van Dinther EAW, van Hout-Kuijer MA, Cerundolo V, Figdor CG, Co-delivery of PLGA encapsulated invariant NKT cell agonist with antigenic protein induce strong T cell-mediated antitumor immune responses, OncoImmunology5 (1) (2016), e1068493. [PubMed: 26942088]

[32]. Hamdy S, Molavi O, Ma Z, Haddadi A, Alshamsan A, Gobti Z, Elhasi S, Samuel J, Lavasanifar A, Co-delivery of cancer-associated antigen and Toll-like receptor 4 ligand in PLGA nanoparticles induces potent CD8+ T cell-mediated anti-tumor immunity, Vaccine26 (39) (2008) 5046–5057. [PubMed: 18680779]

[33]. Liu J, Liu X, Han Y, Zhang J, Liu D, Ma G, Li C, Liu L, Kong D, Nanovaccine incorporated with hydroxychloroquine enhances antigen cross-presentation and promotes antitumor immune responses, ACS Appl. Mater. Interfaces10 (37) (2018) 30983–30993. [PubMed: 30136844]

[34]. Kavunja HW, Lang S, Sungsuwan S, Yin Z, Huang X, Delivery of foreign cytotoxic T lymphocyte epitopes to tumor tissues for effective antitumor immunotherapy against pre-established solid tumors in mice, Cancer Immunol. Immunother66 (4) (2016) 1–10. [PubMed: 27714433]

[35]. Liu H, Moynihan KD, Zheng Y, Szeto GL, Li AV, Huang B, Van Egeren DS, Park C, Irvine DJ, Structure-based programming of lymph-node targeting in molecular vaccines, Nature507 (7493) (2014) 519–522. [PubMed: 24531764]

[36]. Chen Q, Chen M, Liu Z, Local biomaterials-assisted cancer immunotherapy to trigger systemic antitumor responses, Chem. Soc. Rev48 (22) (2019) 5506–5526. [PubMed: 31589233]

[37]. Chen Q, Xu L, Liang C, Wang C, Peng R, Liu Z, Photothermal therapy with immune-adjuvant nanoparticles together with checkpoint blockade for effective cancer immunotherapy, Nat. Commun7 (1) (2016) 13193. [PubMed: 27767031]

[38]. Chen Q, Wang C, Zhan Z, He W, Cheng Z, Li Y, Liu Z, Near-infrared dye bound albumin with separated imaging and therapy wavelength channels for imaging-guided photothermal therapy, Biomaterials35 (28) (2014) 8206–8214. [PubMed: 24957292]

[39]. Yang K, Hu L, Ma X, Ye S, Cheng L, Shi X, Li C, Li Y, Liu Z, Multimodal imaging guided photothermal therapy using functionalized graphene nanosheets anchored with magnetic nanoparticles, Adv. Mater24 (14) (2012) 1868–1872. [PubMed: 22378564]

[40]. Yang K, Zhang S, Zhang G, Sun X, Lee S-T, Liu Z, Graphene in mice: ultrahigh in vivo tumor uptake and efficient photothermal therapy, Nano Lett. 10 (9) (2010) 3318–3323. [PubMed: 20684528]

[41]. Tomayko MM, Tomayko MM, Reynolds CP, Reynolds CP, Determination of subcutaneous tumor size in athymic (nude) mice, Cancer Chemother. Pharmacol24 (3) (1989) 148–154. [PubMed: 2544306]

[42]. Cai JQ, Davison BE, Ganellin CR, Thaisrivongs S, New 3,4-O-isopropylidene derivatives of D-glucopyranosides and L-glucopyranosides, Tetrahedron Lett. 36 (36) (1995) 6535–6536.

[43]. Fife TH, Jao LK, Substituent effects in acetal hydrolysis, J. Org. Chem30 (5) (1965) 1492–1495.

[44]. Karttunen J, Shastri N, Measurement of ligand-induced activation in single viable T cells using the lacZ reporter gene, Proc. Natl. Acad. Sci. U. S. A88 (9) (1991) 3972–3976. [PubMed: 1902576]

[45]. Kattunen J, Sanderson S, Shastri N, Detection of rare antigen-presenting cells by the lacZ T-cell activation assay suggests an expression cloning strategy for T-cell antigens, Proc. Natl. Acad. Sci. U. S. A89 (13) (1992) 6020–6024. [PubMed: 1378619]

[46]. Kasturi SP, Skountzou I, Albrecht RA, Koutsonanos D, Hua T, Nakaya HI, Ravindran R, Stewart S, Alam M, Kwissa M, Villinger F, Murthy N, Steel J, Jacob J, Hogan RJ, García-Sastre A, Compans R, Pulendran B, Programming the magnitude and persistence of antibody responses with innate immunity, Nature470 (7335) (2011) 543–550. [PubMed: 21350488]

[47]. Le Mercier I, Poujol D, Sanlaville A, Sisirak V, Gobert M, Durand I, Dubois B, Treilleux I, Marvel J, Vlach J, Blay J-Y, Bendriss N-V, Caux C, Puisieux I, Goutagny N, Tumor promotion by intratumoral plasmacytoid dendritic cells is reversed by TLR7 ligand treatment, Canc. Res73 (15) (2013) 4629–4640.

[48]. Wang H, Li X, Tse BW-C, Yang H, Thorling CA, Liu Y, Touraud M, Chouane JB, Liu X, Roberts MS, Liang X, Indocyanine green-incorporating nanoparticles for cancer theranostics, Theranostics8 (5) (2018) 1227–1242. [PubMed: 29507616]

[49]. Chen Z, Zhao P, Luo Z, Zheng M, Tian H, Gong P, Gao G, Pan H, Liu L, Ma A, Cui H, Ma Y, Cai L, Cancer cell membrane–biomimetic nanoparticles for homologous-targeting dual-modal imaging and photothermal therapy, ACS Nano10 (11) (2016) 10049–10057. [PubMed: 27934074]

[50]. Jung HS, Verwilst P, Sharma A, Shin J, Sessler JL, Kim JS, Organic molecule-based photothermal agents: an expanding photothermal therapy universe, Chem. Soc. Rev47 (7) (2018) 2280–2297. [PubMed: 29528360]

[51]. Yoon H-J, Lee H-S, Lim J-Y, Park J-H, Liposomal indocyanine green for enhanced photothermal therapy, ACS Appl. Mater. Interfaces9 (7) (2017) 5683–5691. [PubMed: 28152314]

[52]. Zheng M, Zhao P, Luo Z, Gong P, Zheng C, Zhang P, Yue C, Gao D, Ma Y, Cai L, Robust ICG theranostic nanoparticles for folate targeted cancer imaging and highly effective photothermal therapy, ACS Appl. Mater. Interfaces6 (9) (2014) 6709–6716. [PubMed: 24697646]

[53]. Jiang J, Dong LEI, Qin BIN, Shi H, Guo X, Wang YAN, Decreased expression of TLR7 in gastric cancer tissues and the effects of TLR7 activation on gastric cancer cells, Oncol. Lett12 (1) (2016) 631–636. [PubMed: 27347192]

[54]. Clemente T, Dominguez MR, Vieira NJ, Rodrigues MM, Amarante-Mendes GP, In vivo assessment of specific cytotoxic T lymphocyte killing, Methods61 (2) (2013) 105–109. [PubMed: 23454288]

[55]. Cheng L, Wang C, Feng L, Yang K, Liu Z, Functional nanomaterials for phototherapies of cancer, Chem. Rev114 (21) (2014) 10869–10939. [PubMed: 25260098]

[56]. Chen Q, Hu Q, Dukhovlinova E, Chen G, Ahn S, Wang C, Ogunnaike EA, Ligler FS, Dotti G, Gu Z, Photothermal therapy promotes tumor infiltration and antitumor activity of CAR T cells, Adv. Mater31 (23) (2019) 1900192.

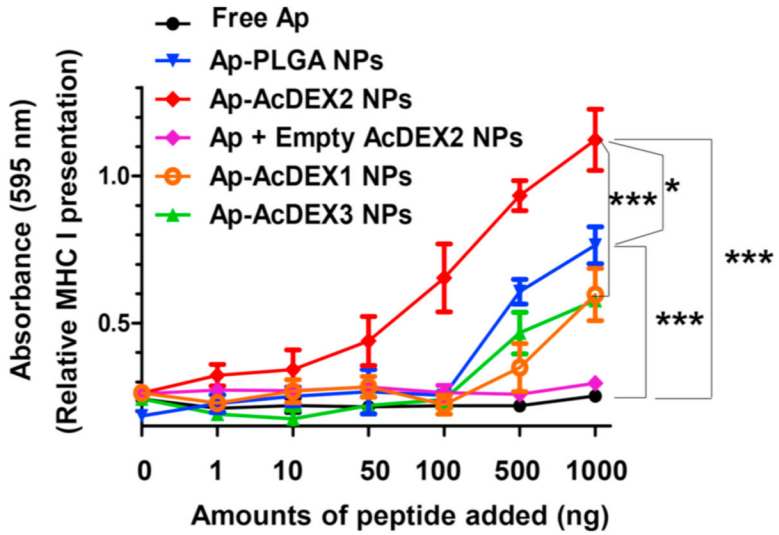

Fig. 1.

MHC-I antigen cross-presentation (B3Z assay) by EL4 lymphoma cells for Ap-containing AcDEX NPs and PLGA NPs. *In vitro* CTL activation study of B3Z T cells co-cultured with EL4 cells treated with free Ap, Ap-AcDEX1 NPs, Ap-AcDEX2 NPs, Ap-AcDEX3 NPs, Ap-PLGA NPs or Ap mixed with empty AcDEX2 NPs. The error bars show the standard error of the mean (s.e.m.) of three replicates. *$p < 0.05$, ***$p < 0.001$. The p values are analyzed by two-way ANOVA (Bonferroni post-test) with GraphPad Prism.

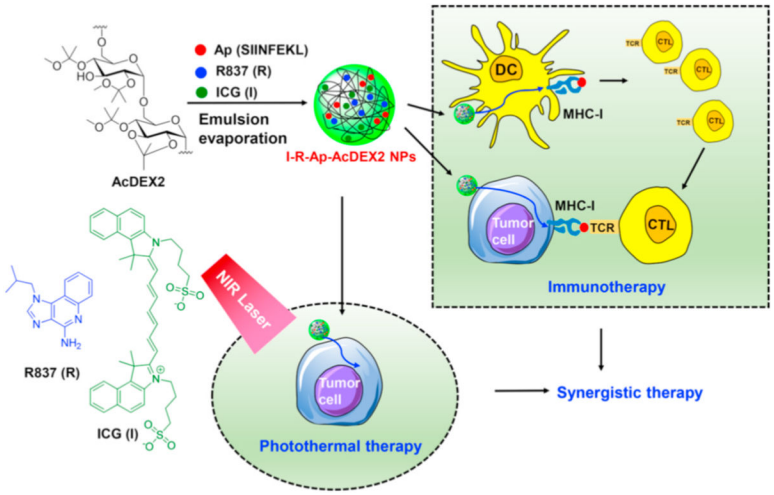

Fig. 2.

Illustration for the design of I-R-Ap-AcDEX2 NPs for synergistic immuno-photothermal therapy against the tumor.

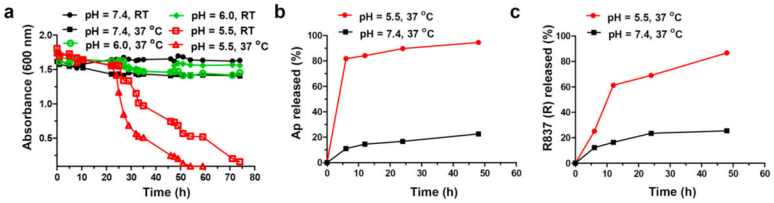

Fig. 3.

pH responsiveness of I-R-Ap-AcDEX2 NPs. (a) Degradation of AcDEX2 NPs at pH values of 7.4, 6.0 or 5.5 at RT and 37 °C in 0.1 M PBS as monitored by UV–Visible absorbance at 600 nm. (b) Ap and (c) R837 release profiles from I-R-Ap-AcDEX2 NPs in PBS with pH 5.5 and 7.4 at 37 °C.

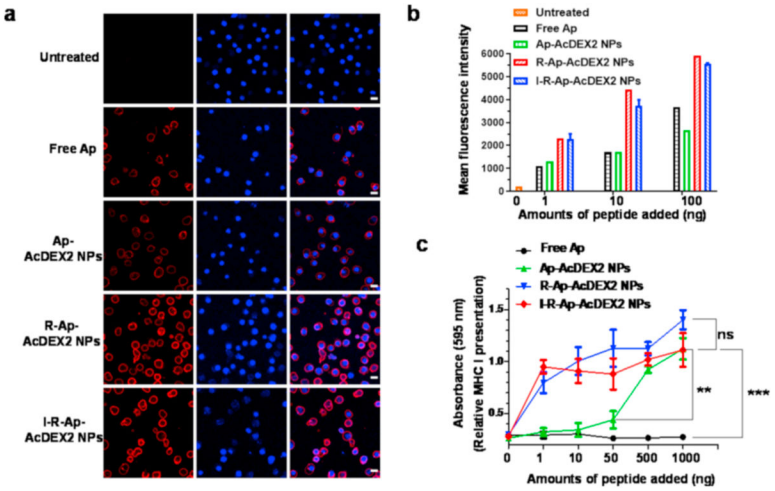

Fig. 4.

Detection of Ap presented by MHC-I of cancer cells. EL4 tumor cells (5×10^5) were incubated with either free Ap, Ap-AcDEX2 NPs, I-R-Ap-AcDEX2 NPs, or R-Ap-AcDEX2 NPs for 6 h. (a) The resulting cells were spiked with PE-labeled anti-mouse H-$2K^b$/SIINFEKL antibody for 30 min, stained with DAPI, and imaged by confocal microscopy. Scale bars: 20 μm. (b) The cells were spiked with PE-labeled anti-mouse H-$2K^b$/SIINFEKL antibody for 30 min and analyzed by flow cytometry. (c) MHC-I antigen presentation (B3Z assay) by EL4 cells. *In vitro* CTL activation study of B3Z T cells co-cultured with EL4 cells following incubation with free Ap, Ap-AcDEX2 NPs, R-Ap-AcDEX2 NPs, or I-R-Ap-AcDEX2 NPs. The error bars show s.e.m. of three replicates. ns: no significant difference, $^{**}p < 0.01$, $^{***}p < 0.001$. The p values are analyzed by two-way ANOVA (Bonferroni post-test) with GraphPad Prism.

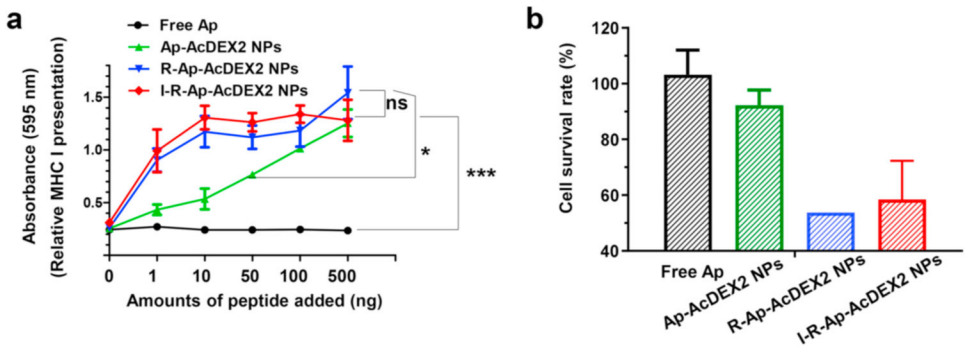

Fig. 5.

CTL activation studies. (a) MHC-I antigen presentation (B3Z assay) by BMDCs. *In vitro* CTL activation study of B3Z T cells co-cultured with BMDCs following incubation with free Ap, Ap-AcDEX2 NPs, R-Ap-AcDEX2 NPs, or I-R-Ap-AcDEX2 NPs. The error bars show s.e.m. of three replicates. ns: no significant difference, $*p < 0.05$, $***p < 0.001$. The p values are analyzed by two-way ANOVA (Bonferroni post-test) with GraphPad Prism. (b) *In vivo* CTL activation study. Mice (1–2 per group) were subcutaneously immunized once with PBS, free Ap, Ap-AcDEX2 NPs, R-Ap-AcDEX2 NPs, or I-R-Ap-AcDEX2 NPs. 7-day later, $CFSE^{hi}$ labeled Ap pulsed target cells were injected into the immunized mice together with $CFSE^{lo}$ labeled control cells. 24 h after cell injection, mice were euthanized, and their splenocytes were prepared for FACS analysis.

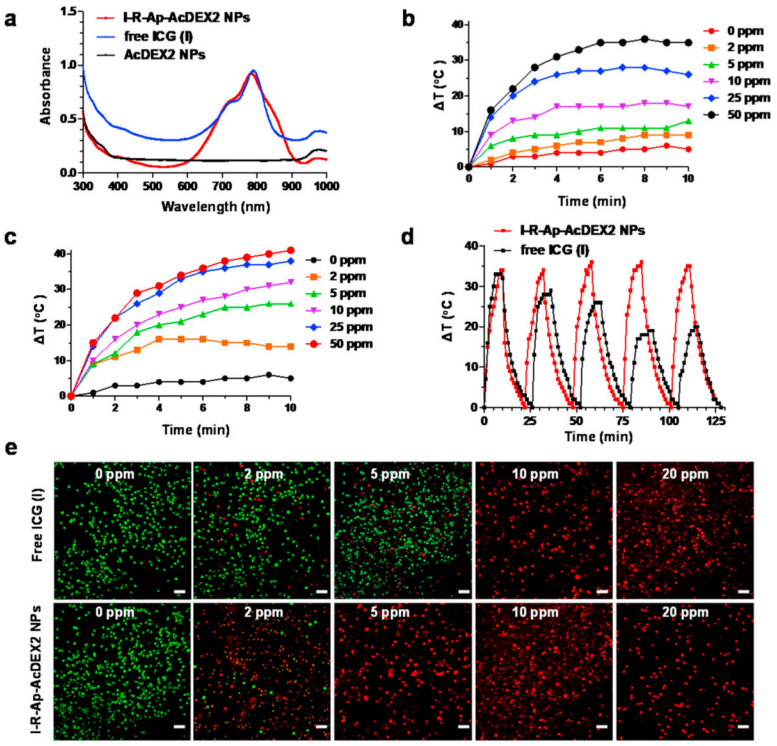

Fig. 6.

Photothermal performance of I-R-Ap-AcDEX2 NPs and free ICG. (a) UV–Visible–NIR absorbance spectra of free ICG, I-R-Ap-AcDEX2 NPs, and AcDEX2 NPs. Temperature variation curves of (b) free ICG and (c) I-R-Ap-AcDEX2 NPs solution under different concentrations (0–50 ppm) in water for 10 min under irradiation with the 808 nm laser (1 W cm^{-2}). (d) Photostability of I-R-Ap-AcDEX2 NPs and free ICG. Heating of a suspension of free ICG (50 ppm) and I-R-Ap-AcDEX2 NPs (50 ppm) in water for five lasers on/off cycles under irradiation with the 808 nm laser (1 W cm^{-2}). (e) Photothermal killing of cancer cells with I-R-Ap-AcDEX2 NPs and free ICG. The NPs or free ICG treated EL4 cells were irradiated with the 808 nm laser (1 W cm^{-2}) for 10 min, stained with PI (dead cells, red) and calcein-AM (live cells, green). Scale bars: 100 μm. (For interpretation of the references to color in this figure legend, the reader is referred to the Web version of this article.)

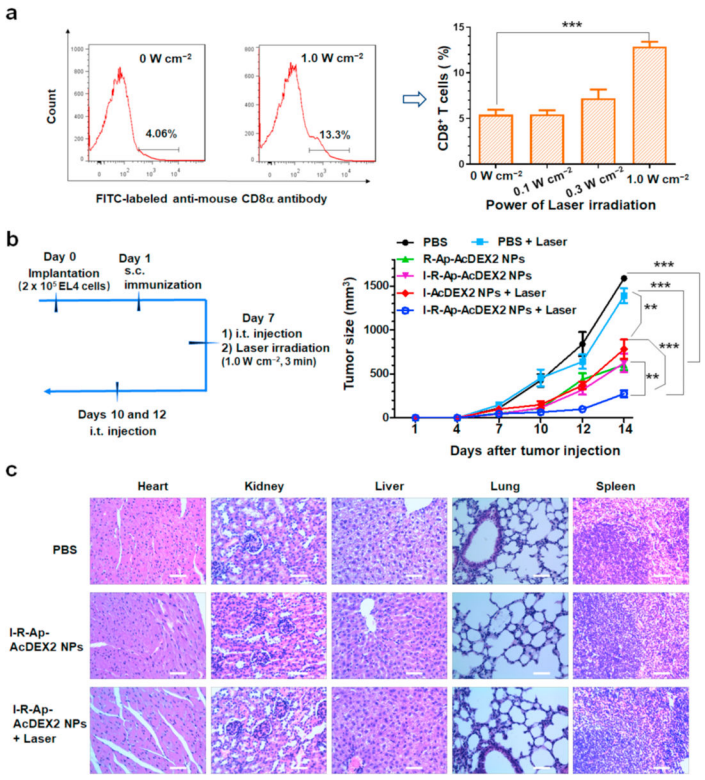

Fig. 7.

I-R-Ap-AcDEX2 NPs can provide effective protection against tumor development in an animal tumor model. (a) Photothermal therapy promotes $CD8^+$ T cell infiltration in the tumor. C57BL/6 mice were subcutaneously injected with EL4 cells (2×10^5) on day 0, subcutaneously immunized on day 1 under the scruff with I-R-Ap-AcDEX2 NPs, intratumorally given one injection with I-R-Ap-AcDEX2 NPs on day 7. The tumors were irradiated with the 808 nm laser at 0, 0.1, 0.3, 1.0 W cm^{-2} for 3 min, respectively. Then, the percentage of $CD8^+$ T cells present in the subcutaneous EL4 tumor was determined by FITC-labeled CD8α antibody staining. (n = 3 mice for each group). ***$p < 0.001$. The p values are analyzed by a two-tailed unpaired Student's t-test with GraphPad Prism. (b) EL4 tumor challenge via intratumoral administration of the NPs. C57BL/6 mice were injected with EL4 cells (2×10^5) by subcutaneous injection on day 0. They were subcutaneously injected on day 1 under the scruff with PBS or the NPs, intratumorally given 3 injections with PBS or the NPs on day 7, 10 and 12. The mice were irradiated for laser-treated groups with the 808 nm laser (1.0 W cm^{-2}, 3 min) only on day 7. (n = 5 mice for each group). ns: no significant difference, **$p < 0.01$, ***$p < 0.001$. The p values are analyzed by two-way ANOVA (Bonferroni post-test) with GraphPad Prism. (c) Cytotoxicity of the NPs by histological analysis. The organs of mice were harvested, sectioned, and stained with hematoxylin/eosin. No lesions were observed from these slides. Scale bars: 200 μm.

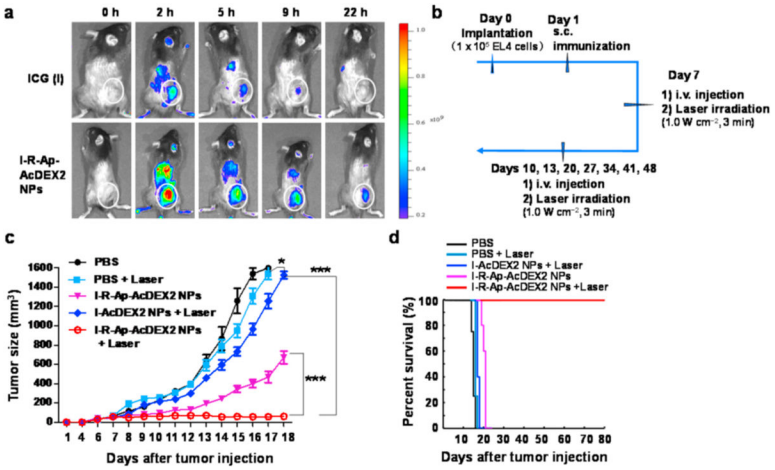

Fig. 8.

Systemic administration of the NPs. (a) Time-lapse illumination of subcutaneous tumors with I-R-Ap-AcDEX2 NPs. C57BL/6 mice bearing subcutaneous tumors were intravenously injected with I-R-Ap-AcDEX2 NPs (1 mg, with 30 μg of ICG in the NPs) or ICG (30 μg) via tail vein and then imaged for *in vivo* NIR fluorescence emission at the indicated time points. Circles indicate the location of tumors. (b–c) EL4 tumor challenge via systemic administration of the NPs. C57BL/6 female mice were inoculated with EL4 cells (1×10^5) on day 0 by subcutaneous injection, subcutaneously immunized on day 1 under the scruff with PBS or the NPs, intravenously given a total of three injections with PBS or the NPs on days 7, 10 and 13. For laser-irradiated groups, the mice were irradiated with the 808 nm laser (1.0 W cm^{-2}, 3 min) 2 h after injection of the NPs or PBS on days 7, 10 and 13, respectively. Five more intravenous injections of I-R-Ap-AcDEX2 NPs and laser irradiations were given in the group (I-R-Ap-AcDEX2 NPs + Laser). (n = 5 mice for each group). ns: no significant difference, $*p < 0.05$, $***p < 0.001$. The *p* values are analyzed by two-way ANOVA (Bonferroni post-test) with GraphPad Prism. (d) The survival curve of EL4 tumor challenge by systemic administration.

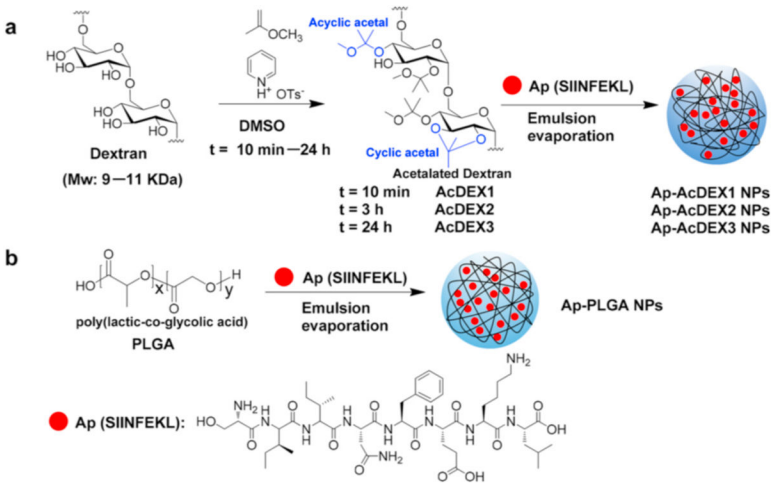

Scheme 1.

Synthesis of Ap-AcDEX1 NPs, Ap-AcDEX2 NPs, Ap-AcDEX3 NPs, and Ap-PLGA NPs.